# Chapter 138
# Finite Element Simulation and Experimental Investigation on the Residual Stress Redistribution Induced Distortion During Blade Machining


**Kunyang Lin, Xiaofei Ma, and Wenhu Wang**

**Abstract** Residual stresses play a dominant role on the machining distortion problem. The effect of cutting parameters on the residual stress have been studied by many researchers. However, the redistribution of initial residual stress during machining is always been ignored. In this paper, a finite element model is established to investigate the stress redistribution coupling initial residual stress and cutting residual stress during the blade machining process. The model contains two parts: the heat treatment model and the machining model. The initial residual stress field by the quenching process is established in the heat treatment model. Then the machining process is simulated as the range of roughing machining, semi finishing and finishing. In addition, a cutting experiment is conducted to study the distribution of cutting residual stress on the blade surface. The result shows that the initial stress is more significant in the rough machining stage and the cutting residual stresses play a dominated role in the finishing machining stage of blade. The result is helpful to understand the redistribution mechanic during machining process better.

**Keywords** Residual stress · Machining · Finite element simulation · Blade

## 138.1 Introduction

Machining distortion is one of the serious problems in the manufacture industry, especially for the thin-walled components [1, 2]. Residual stresses induced machining distortion has been considered to be the main factor of machining distortion. During

K. Lin · X. Ma (✉)
China Academy of Space Technology (Xi'an), Xi'an 710100, China
e-mail: maxf041600@sina.com

K. Lin
e-mail: linkunyang@126.com

W. Wang
School of Mechanical Engineering, Northwestern Polytechnical University, Xi'an 710072, China
e-mail: npuwwh@nwpu.edu.cn



J. Tan (ed.), *Advances in Mechanical Design*, Mechanisms and Machine Science 111,
https://doi.org/10.1007/978-981-16-7381-8_138

the machining process, the blank initial residual stress and machining induced residual stress may redistribute and destroy the equilibrium state of residual stress field, which induces the machining distortion problem. In order to overcome the machining distortion problem, researchers have developed different methods to predict or control the machining distortion of thin-walled components [3–5].

As the high cost of machining experiments, researchers have established a variety of prediction models of residual stress and machining distortion with the help of different numerical tools. Tang et al. [6] used ABAQUS commercial finite element analysis software, combined with metal cutting principle, established a distortion prediction finite element model considering the coupling effects of cutting residual stress and clamping force. Cerutti and Mocellin [7] developed a special numerical tool to simulate the change of workpiece deformation characteristics with material removal, and predicted the influence of cutting sequence, initial residual stress field and clamping scheme on the workpiece shape and dimensional accuracy. Based on the secondary development interface of ABAQUS software, Ma et al. [8] simulated the evolution of residual stress in the cutting process by using the birth and death element method and analyzed the deformation of thin-walled frame parts under the coupling of initial residual stress and cutting residual stress. D'alvise et al. [9] proposed that the "level set" method can be used to simulate the initial residual stress and the machining deformation caused by the cutting residual stress. Compared with the traditional thermal mechanical coupling simulation method, this method can effectively reduce the simulation time. Brinksmeier et al. [10] systematically studied the deformation problem in gear machining and pointed out that the redistribution of blank residual stress caused by material removal method was the main reason for gear machining deformation, and the optimization of material removal method can greatly improve the machining deformation problem.

In addition to the machining distortion prediction method, many researchers have studied to control the machining parameters and tool parameters to reducing machining distortion. Li et al. [11] designed several groups of cutting experiments to study the effects of cutting parameters, tool diameter, tool overlap coefficient, cutting path and clamping mode on the residual stress and machining distortion under the condition of high-speed milling. Based on the experiment results, they put forward the method of controlling the cutting depth in different stages for subsequent machining. Masoudi et al. [12] studied the cutting force and cutting temperature of Al7050T66 aluminum alloy thin-walled cylinder processed by cemented carbide tool and PCD tool. The researches show that the distortion of thin-walled cylinder increases with the increase of cutting force and cutting temperature, and the influence of cutting force on the distortion is more significant than that of cutting temperature. PCD tool can help to reduce the cutting distortion problem.

Although some studies have analyzed the machining distortion, there is not enough comprehensive study on the main cause of machining distortion of thin-walled component. The redistribution process of initial residual stress and machining induced residual stresses on thin-walled component distortion has not been fully explored. More researches are required to understand how the residual stress induces

**Table 138.1** Typical mechanical parameters of $TiB_2$/7050 Al composite at room temperature

| Density ($g/cm^3$) | Poisson's ratio | Elastic modulus (GPa) | Yield strength (MPa) | Elongation (%) | Coefficient of thermal expansion ($K^{-1}$) |
|---|---|---|---|---|---|
| 2.90 | 0.33 | 78 | 630 | 6 | $2.1 \times 10^{-6}$ |

the machining distortion problem. In this research, a finite element model is established to simulate the origin process of initial residual stress and the redistribution of initial residual stress and cutting residual stress during the machining process of blade.

## 138.2 Finite Element Simulation and Experiments

### *138.2.1 Materials*

The workpiece material used in this work is named as in situ 6 wt% $TiB_2$ particle reinforced 7050 aluminum meal matrix composites (shorted as $TiB_2$/7050 Al composites). The $TiB_2$/7050 Al composites were prepared via mixed salts reaction of $K_2TiF_6$ and $KBF_4$. Detailed preparing procedures can be found in the Ref. [13]. By the mixed salt reaction technique, the $TiB_2$ reinforcement particles are homogeneous distributed with the particle size ranging from 20 to 500 nm [14]. The mechanical parameters of $TiB_2$/7050 Al composite at room temperature is shown in Table 138.1.

### *138.2.2 FEM Model*

In this work, the finite element model consists of two parts, the heat treatment model and the machining model.

#### 138.2.2.1 Heat Treatment Model

The initial residual stress of $TiB_2$/7050 Al composites blank derived from the heat treatment model, which consisted of the quenching and the pre-stretching process. In the material preparing stage, the $TiB_2$/7050 composites were homogenized at 470 °C for 24 h and then extruded. The solution treatment was carried out at 477 °C for 190 min followed by a water quenching process. In order to reduce the quenching stress, 1.5% pre-stretching was performed along the longitudinal direction. The dimension of specimens used in this study is 169.7 mm × 84.4 mm × 64.4 mm.

**Table 138.2** Johnson–Cook parameters for $TiB_2$/7050 composites

| *A* | *B* | *C* | *m* | *n* |
|---|---|---|---|---|
| 594 | 446.4538 | 0.0157 | 1.364 | 0.4655 |

An elastic-perfectly plastic FEA model of the quenching process is performed using a commercial software ABAQUS/Standard.

The Johnson–Cook constitutive model is used to describe the stress–strain responses of $TiB_2$/7050 Al composites under different strain, strain rate and temperature with strain hardening and non-liner material properties, which can be expressed as Eq. (138.1):

$$\sigma = \left[A + B(\varepsilon)^n\right]\left[1 + C\ln\left(\frac{\dot{\varepsilon}}{\dot{\varepsilon}_0}\right)\right]\left[1 - \left(\frac{T - T_0}{T_{melt} - T_0}\right)^m\right] \tag{138.1}$$

where $\sigma$ is the flow stress, $\boldsymbol{\varepsilon}$, $\dot{\varepsilon}$, $\dot{\varepsilon}_0$ means the effective plastic strain, the effective strain rate and the reference strain rate ($10^{-3}$/s in this study) respectively. $T_0$ and $T_{melt}$ stands for the room temperature and material melting temperature, respectively. The parameters *A*, *B*, *C*, *m*, *n* for $TiB_2$/7050 Al composites are defined in Table 138.2.

#### 138.2.2.2 Machining Model

The geometry of the blade used in this study is shown in Fig. 138.1. The length of the blade is 120 mm with the maximum thickness of 3.46 mm. The material of the blade is $TiB_2$/7050 Al composites. During the machining process, the material is removed in the roughing machining, semi finishing and finishing stage. The birth and death element method is used to simulate the material removal process.

Hexahedral solid grid element (C3D8R) is used to calculate the initial residual stress field of the blank, as shown in Fig. 138.2, with a total of 122,034 nodes and 114,240 elements. The blade is meshed by the tetrahedral solid element (C3D10) with 20,136 nodes and 11,286 elements.

### *138.2.3 Machining of Blades and Measuring of Residual Stress*

The cutting experiment is conducted on a VMC-850 three-coordinate vertical CNC milling machine as shown in Fig. 138.3. The material of the blade is $TiB_2$/7050 Al composite and the size of the blank is the same as the simulation model. After the machining process, the surface residual stress is measuring by PROTO-LXRD MG2000 residual stress measuring system. The detailed parameters are described in Table 138.3. After the surface residual stress measurement, the surface was stripped

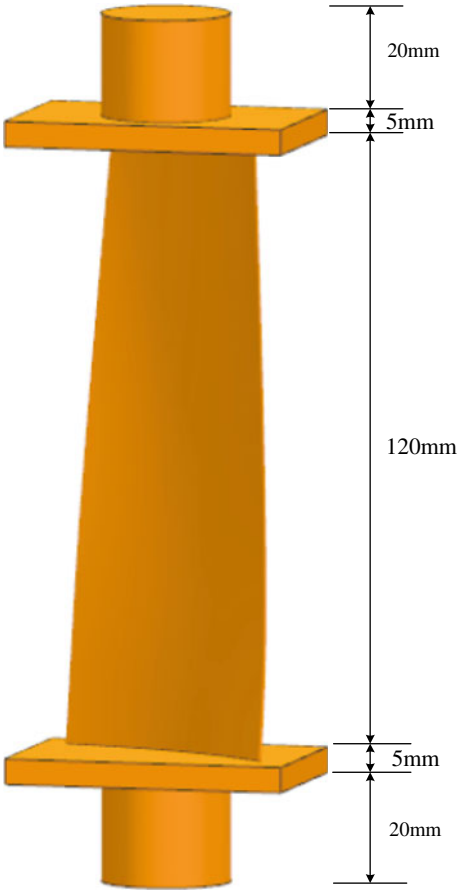


**Fig. 138.1** Design of the blade

applying electro-chemical polishing method to measure the subsurface residual stress. The chemical solution used was supersaturated slat water. Each specimen was polished over 200 μm until the residual stress closed to the material's basis state.

## 138.3 Results and Discussions

### *138.3.1 Initial Residual Stress Redistribution During Machining*

The simulated initial residual stresses of blank after heat treatment in different directions are shown in Fig. 138.4. The blank presents the residual stress distribution of

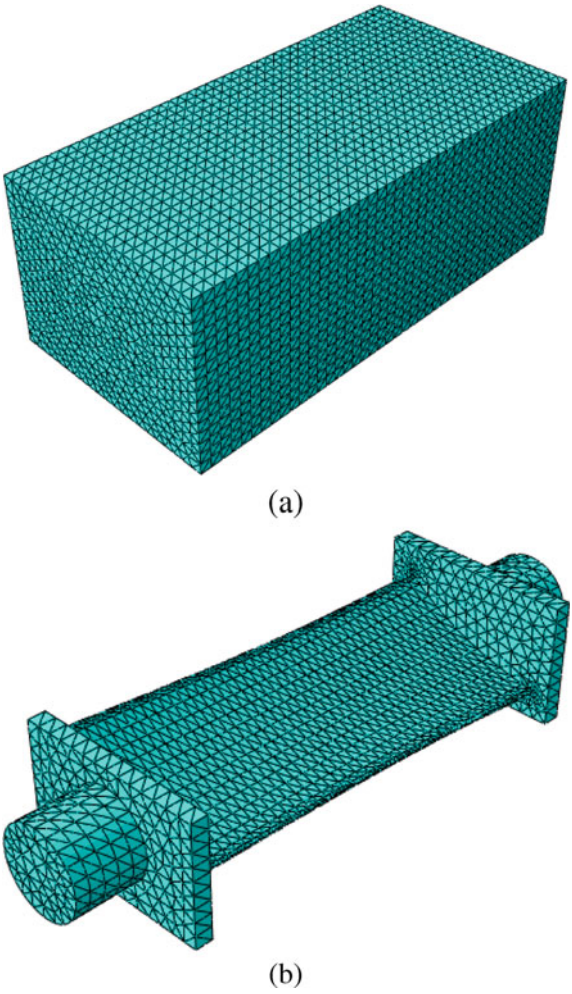


**Fig. 138.2** Finite element model: **a** blank, **b** blade

external compressive stresses and internal tensile stresses. The normal stress in the $x$ direction $\sigma_{xx}$ ranges form –76 to 35 MPa, in $y$ direction the normal stress $\sigma_{yy}$ ranges from –69 to 20 MPa, in $z$ direction the normal stress $\sigma_{zz}$ ranges from –77 to 33 MPa. The maximum compressive stress amplitude is obviously larger than the maximum tensile stress amplitude, which is due to the temperature gradient of the workpiece outer surface is greater than that of the core during heat treatment, and the thermo-plastic deformation of the surface material is greater than that of the inner material, thus forming a higher residual stress amplitude on the surface.

The evolution processes of the stress field with the removal of material are shown in Fig. 138.5. In Fig. 138.5a, the axles at both ends are turned for positioning and datum in the subsequent milling process. After turning the axles, the workpiece still keeps symmetrically. As the amount of removed material is little, the workpiece

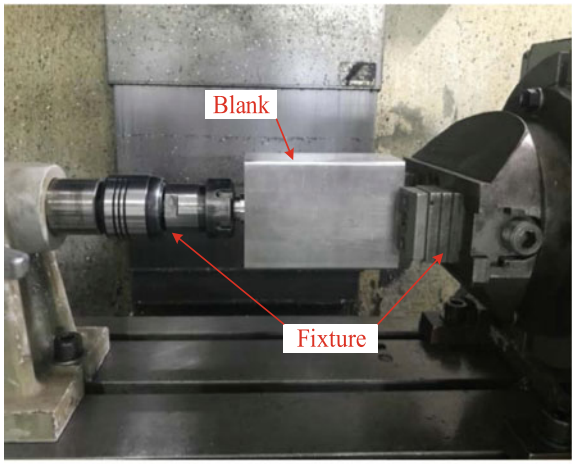


**Fig. 138.3** Experimental setup

**Table 138.3** Conditions for measuring residual stress

| Measuring method | Iso-inclining method with fixed ψ |
|---|---|
| Diffraction plane (*hkl*) | (311) |
| Characteristic X-ray | Co-Kα |
| Tube voltage (kV) | 25 |
| Diffraction angle (°) | 149 |
| Number of exposures | 10 |
| Tube current (mA) | 20 |
| Exposure time (s) | 1 |
| ψ angles (°) | 40.5, 35.51, 31, 24.25, 16.88, 15.5, 14.12, 6.75, 0, −4.51, −9.50 |

after turning still has good stiffness and the internal stress field of the workpiece still maintains a nearly symmetrical distribution state as shown in Fig. 138.5b.

After rough machining as shown in Fig. 138.5c, a large number of materials is removed, and the workpiece becomes thinner significantly. Due to the bending and twisting structural characteristics of the blade, the stress field cannot maintain a symmetrical distribution state. In order to form a new equilibrium state, the internal stress of the workpiece redistributes. The initial residual stresses of the blank mainly come from the heat treatment process. The distribution of the initial residual stress on the outer surface of the blank has a large stress gradient, and the stress gradient of the internal stress field tends to be gentle. When the outer material is removed, the area with large residual stresses is removed. In this process, the residual stress is significantly reduced and the maximum stress reduced from 63.89 to 28.2 MPa. After rough machining, the stress field in the blank becomes unsymmetrical distribution state.

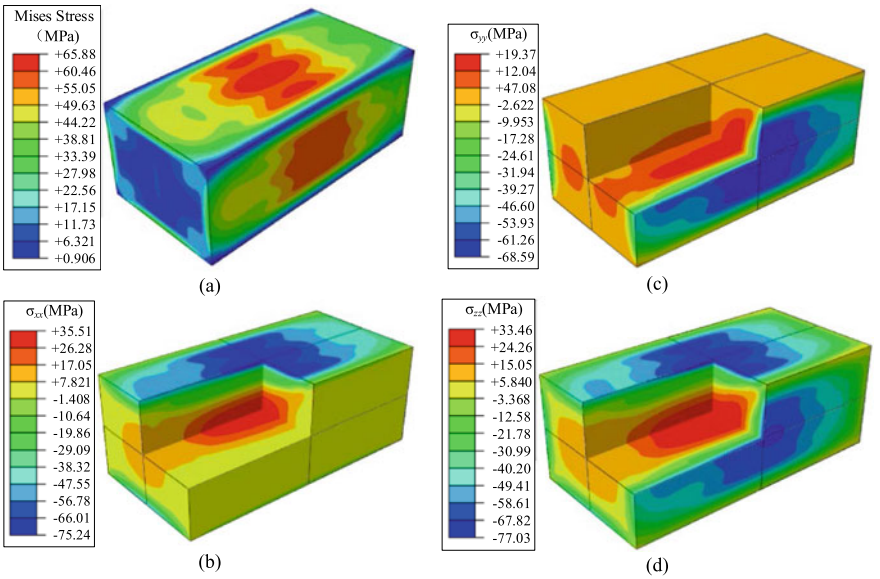


**Fig. 138.4** Initial residual stress field of blank: **a** Mises stress field, **d** residual stress in the x direction, **b** residual stress in the y direction, **c** residual stress in the z direction

The semi finishing and finishing process is shown in Fig. 138.5d, e, respectively. The material removal allowance in the semi finishing and finishing process is 1 mm and 0.5 mm respectively. It seems that the semi finishing and finishing machining have little effect on the initial residual stress.

Figure 138.5f shows the balance state of the blade after machining. The maximum stress in the workpiece is 10.48 MPa and the residual stress in blade body is generally lower than 10 MPa. Considering that the blade is thin after finishing and the cutting residual stress on the surface is usually larger than the initial residual stress due to the drastic cutting thermal and force coupling effect, it can be inferred that the cutting residual stress will play a dominant role in the distortion of the workpiece during finishing compared with the initial residual stress in the workpiece.

### *138.3.2 Machining Distortion Considering Initial Residual Stress and Cutting Residual Stress*

After the machining process, the surface residual stress is measured on the convex and concave surface. The distribution of measurement points was shown in Fig. 138.6. B1, B2 and B3 were the measurement points on the convex surface, while P1, P2 and P3 were the measurement points on the concave surface. At each point, the cutting residual stress along $x$ direction and $y$ direction are measured, respectively. In this

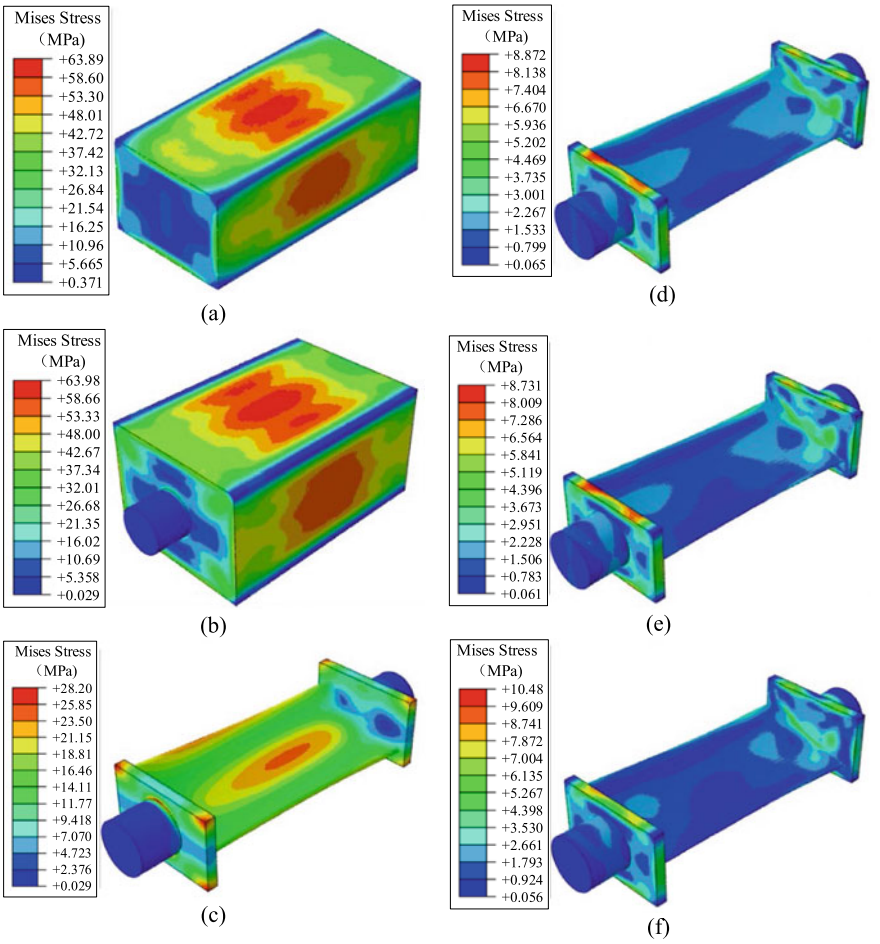


**Fig. 138.5** Evolution of initial residual stress field with the removal of material: **a** initial residual stress field of blank, **b** stress field after turning the axles, **c** stress field after rough machining, **d** stress field after semi finishing, **e** stress field after finishing, **f** stress equilibrium state after material removal

work, *y* direction is the tool feed direction, and *x* direction is perpendicular to the tool feed direction. The results of measured surface cutting residual stress on the convex surface and concave surface are shown in Figs. 138.7 and Fig. 138.8 respectively.

With the results of initial residual stress field and cutting residual stress, the machining distortion of blade caused by initial residual stress, machining distortion caused by cutting residual stress, machining distortion of blade under the coupling of blank initial residual stress and cutting residual stress are calculated respectively, while the results are shown in Fig. 138.9. As shown in the figures, the maximum distortion caused by initial residual stress is 0.084 mm. The maximum deformation

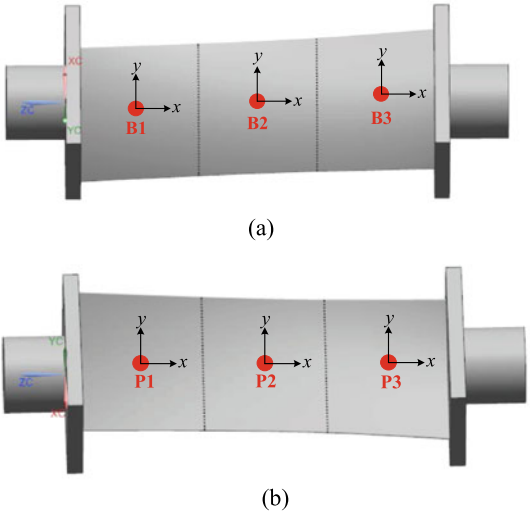


**Fig. 138.6** Measuring point of residual stress on the blade surface after finishing: **a** convex surface, **b** concave surface

caused by cutting residual stress is 0.126 mm. Under the combined action of initial residual stress and cutting residual stress, the maximum deformation of the blade after machining is 0.13 mm. It can be seen that for thin-walled blade, the influence of initial residual stress on machining deformation is little, and the influence of cutting residual stress on machining deformation is more significant. From the perspective of maximum deformation, the contribution rate of cutting residual stress to machining deformation is 97%, and the contribution rate of initial residual stress to machining deformation is 3%. Under the coupling effect of initial residual stress and cutting residual stress, the blade appears obvious deflection deformation along the blade axis. The distortion at the blade tip is larger than the distortion at the blade root. The simulation result agree well with the actual machining result. During the machining process, the equilibration of initial residual stress field is broken with the removal of material. In order to re-equilibrate the residual stress field, the blade is deformed with the redistribution of initial residual stress and cutting residual stress. However, for the thin walled blade, the cutting residual stress induced distortion is larger than the initial residuals stress. This is due to the fact that the residual stress amplitude of cutting residual stress is larger than the initial residual stress. In addition, the cutting residual stress depth is usually lower than 200um which makes higher stress gradient beneath the machined surface and induces unbalanced moment. In order to reduce the machining distortion problem during the machining of $TiB_2$/7050 Al composite blade, the cutting parameters should be well optimized to reduce the cutting residual stress.

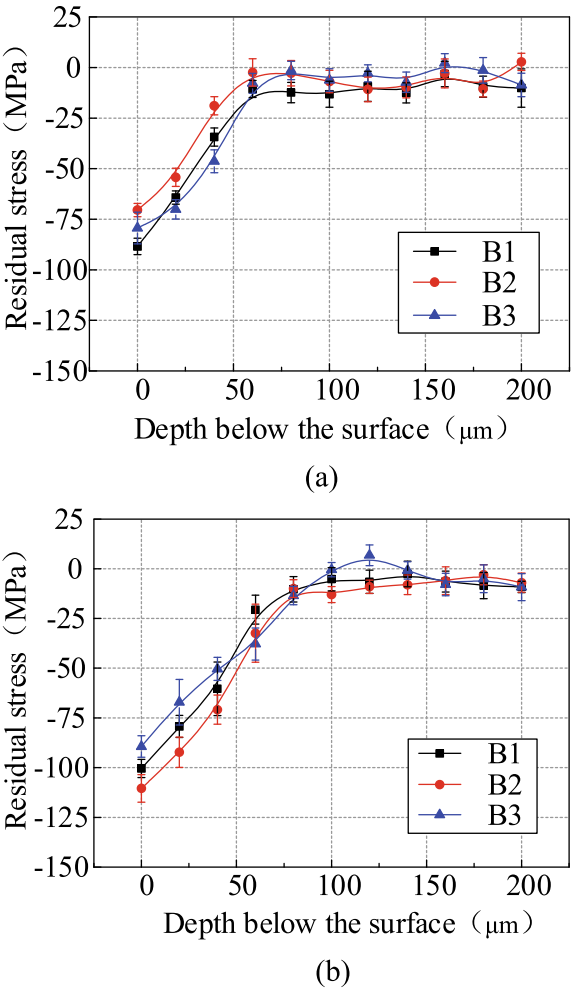


**Fig. 138.7** Cutting residual stress on the convex surface points: **a** *x* direction, **b** *y* direction

## 138.4 Conclusions

In this work, a finite element model is established to study the residual stress redistribution and machining distortion caused by the combination of initial residual stress and cutting residual stress during the machining of $TiB_2$/7050 Al composite blade. The main conclusions are drawn as below:

(1) The initial residual stress of $TiB_2$/7050 Al composite blank shows a distribution state of external compressive stress and internal tensile stress. Due to the existence of $TiB_2$ particles, the cutting residual stress on the machined surface is always compressive. With the increase of depth, the surface cutting residual stress decreases gradually.

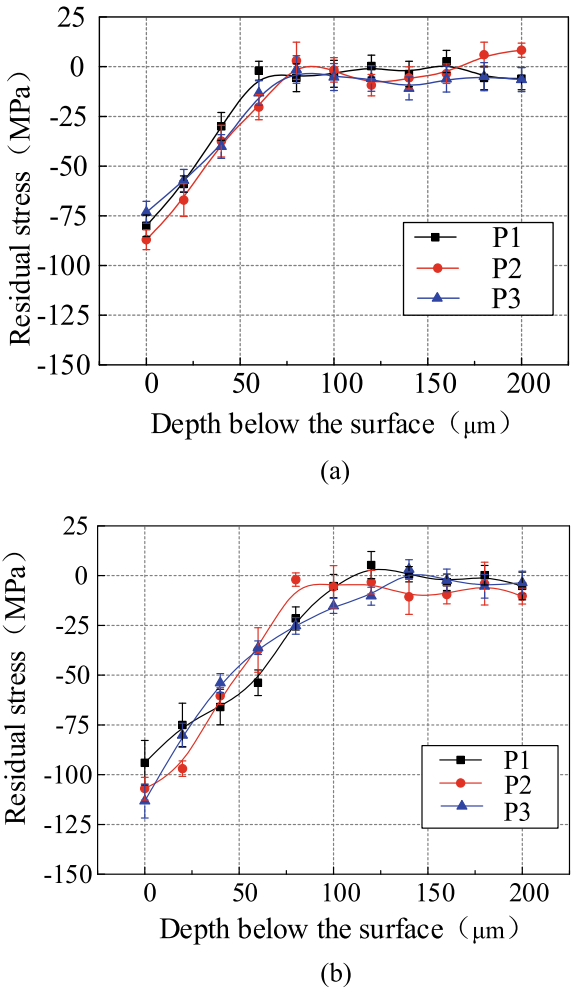


**Fig. 138.8** Cutting residual stress on the concave surface points: **a** *x* direction, **b** *y* direction

(2) The mechanism of residual stress redistribution is analyzed. Large amount of materials is removed during the process of rough machining process, while internal residual stress field changes dramatically and destroyed the equilibration of residual stresses field. In the finishing process, the initial stress has little effect on the residual stress field and the surface state is mainly effected by the cutting residual stress.

(3) The effects of initial residual stress and cutting residual stress on the machining distortion of $TiB_2$/7050 Al composite blade are studied. The contribution rate of cutting residual stress to machining distortion is 97%, and the contribution rate of initial residual stress to machining deformation is 3%. The machining parameters should be well optimized to minimize the machining distortion.

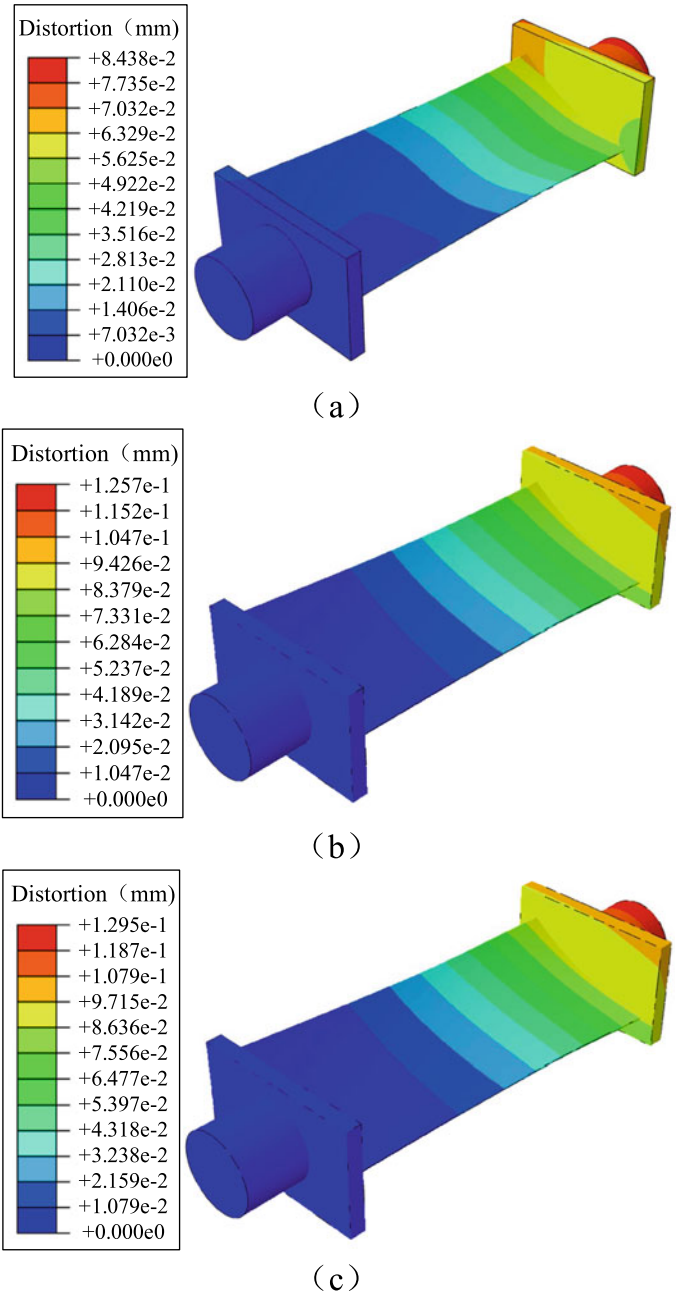


**Fig. 138.9** Simulated distortion result of the blade: **a** distortion by the initial residual stress, **b** distortion by the cutting residual stress, **c** distortion considering both initial residual stress and cutting residual stress

**Acknowledgements** This project is supported by the National Natural Science Foundation of China (Grant No. 51475374) and the China Postdoctoral Science Foundation (Grant No. 2021M703492).

## References

1. Sim, W.-M.: Challenges of residual stress and part distortion in the civil airframe industry. Int. J. Microstruct. Mater. Prop. **5**(4–5), 446–455 (2010)
2. Li, X., et al.: Machining deformation of single-sided component based on finishing allowance optimization. Chin. J. Aeronaut. (2019)
3. Hao, X., et al.: A part deformation control method via active pre-deformation based on online monitoring data. Int. J. Adv. Manuf. Technol. **104**(5), 2681–2692 (2019)
4. Afazov, S., et al.: Distortion prediction and compensation in selective laser melting. Addit. Manuf. **17**, 15–22 (2017)
5. Huang, X.M., Sun, J., Li, J.F.: Finite element simulation and experimental investigation on the residual stress-related monolithic component deformation. Int. J. Adv. Manuf. Technol. **77**(5–8), 1035–1041 (2015)
6. Tang, Z.T., et al.: Machining deformation prediction for frame components considering multifactor coupling effects. Int. J. Adv. Manuf. Technol. **68**(1), 187–196 (2013)
7. Cerutti, X., Mocellin, K.: Parallel finite element tool to predict distortion induced by initial residual stresses during machining of aeronautical parts. Int. J. Mater. Form. **8**(2), 255–268 (2014)
8. Ma, Y., et al.: Modeling of machining distortion for thin-walled components based on the internal stress field evolution. Int. J. Adv. Manuf. Technol. (2019)
9. D'Alvise, L., et al.: Modelling of part distortion due to residual stresses relaxation: an aeronautical case study. Procedia CIRP **31**, 447–452 (2015)
10. Brinksmeier, E., et al.: Distortion minimization of disks for gear manufacture. Int. J. Mach. Tools Manuf **51**(4), 331–338 (2011)
11. Li, B.Z., et al.: Effects of depth of cut on the redistribution of residual stress and distortion during the milling of thin-walled part. J. Mater. Process. Technol. **216**, 223–233 (2015)
12. Masoudi, S., et al.: Effect of machining-induced residual stress on the distortion of thin-walled parts. Int. J. Adv. Manuf. Technol. **76**(1–4), 597–608 (2015)
13. Geng, J., et al.: Microstructural and mechanical anisotropy of extruded in-situ $TiB_2$/2024 composite plate. Mater. Sci. Eng., A **687**, 131–140 (2017)
14. Tang, Y., et al.: Quantitative study of particle size distribution in an in-situ grown Al–$TiB_2$ composite by synchrotron X-ray diffraction and electron microscopy. Mater. Charact. **102**, 131–136 (2015)

**Kunyang Lin** born in 1992, is currently an engineer at China Academy of Space Technology in Xi'an, China. He received his doctor degree in Northwestern Polytechnical University. His research interests include orbital additive manufacturing technology and precision manufacturing technology.

**Xiaofei Ma** born in 1980, is currently a professor at China Academy of Space Technology in Xi'an, China. His research interests include space deployable structure and large space mesh antenna.

**Wenhu Wang** born in 1965, is currently a professor at Northwestern Polytechnical University, China. His research interests is precision manufacturing technology.